https://doi.org/10.1093/plphys/kiad656 PLANT PHYSIOLOGY 2024: 194: 2600–2615

Plant Physiology®

Research Article

Starch phosphorylation regulates starch granule morphological homogeneity in *Arabidopsis thaliana*

Xiaoping Li,[1] **Abubakar Musa Ahmad**,[1] **Yuyue Zhong**,[2] **Li Ding**,[2] **Andreas Blennow**[2] **and Joerg Fettke**[1,*]

1 Biopolymer Analytics, Institute of Biochemistry and Biology, University of Potsdam, Potsdam-Golm 14776, Germany
2 Department of Plant and Environmental Sciences, Faculty of Science, University of Copenhagen, Frederiksberg C 1871, Denmark

*Author for correspondence: fettke@uni-potsdam.de
The author responsible for distribution of materials integral to the findings presented in this article in accordance with the policy described in the Instructions for Authors (https://academic.oup.com/plphys/pages/General-Instructions) is: Joerg Fettke (fettke@uni-potsdam.de).

Abstract

Starch granule morphological homogeneity presents a gap in starch research. Transitory starch granules in wild-type plants are discoid, regardless of species. Notably, while the shape of starch granules can differ among mutants, it typically remains homogeneous within a genotype. We found an *Arabidopsis thaliana* mutant, *dpe2sex4*, lacking both the cytosolic disproportionating enzyme 2 (DPE2) and glucan phosphatase SEX4, showing an unprecedented bimodal starch granule diameter distribution when grown under a light/dark rhythm. *dpe2sex4* contained 2 types of starch granules: large granules and small granules. In contrast to the double starch initiation in wheat (*Triticum aestivum*) endosperm, where A-type granules are initiated first and B-type granules are initiated later, *dpe2sex4* small and large granules developed simultaneously in the same chloroplast. Compared with the large granules, the small granules had more branched amylopectin and less surface starch-phosphate, thus having a more compact structure that may hinder starch synthesis. During plant aging, the small granules barely grew. In in vitro experiments, fewer glucosyl residues were incorporated in small granules. Under continuous light, *dpe2sex4* starch granules were morphologically homogeneous. Omitting the dark phase after a 2-wk light/dark cycle by moving plants into continuous light also reduced morphological variance between these 2 types of granules. These data shed light on the impact of starch phosphorylation on starch granule morphology homogeneity.

Introduction

Transitory starch is an essential carbohydrate stored in the chloroplasts of vascular plants and plays a crucial role in plant metabolism. Starch is accumulated in the form of insoluble semicrystalline granules. In *Arabidopsis thaliana*, each chloroplast contains 3 to 7 discoid starch granules (Streb and Zeeman 2012; Mérida and Fettke 2021). There are reports of mutants with altered starch granule morphology, such as the round granules in *ss4* and *dpe2* (starch synthase 4 [SS4], EC: 2.4.1.21; cytosolic disproportionating enzyme 2 [DPE2], EC: 2.4.1.25; Malinova et al. 2017; Mérida and Fettke 2021), the elongated flattened granules in *ptst2* (protein targeting to starch; Seung et al. 2017), and the larger granules with irregular edges in *sex1-8* (glucan, water dikinase [GWD], EC 2.7.9.4; Malinova and Fettke 2017). Intriguingly, although the morphology of starch granules in different mutants changes, the shape of starch granules remains homogeneous (Vandromme et al. 2019; Mérida and Fettke 2021). Moreover, starch granules within the same plant differ in size rather than in shape (Grange et al. 1989; Santacruz et al. 2004). It is unknown how plants regulate this homogeneity of starch granule morphology.

Starch comprises 2 types of polyglucan—amylopectin and amylose—whose glucosyl units are both connected by α-1,4

Received October 09, 2023. Accepted November 13, 2023. Advance access publication December 7, 2023

Open Access

glycosidic linkages and branched by α-1,6 links. Amylopectin is a highly branched polysaccharide that typically accounts for more than 75% of the starch granule mass. Adjacent glucan chains with the same branching in the granule form double helices and align into the crystalline lamellae, with branching points clustered into amorphous lamellae. This alternation of the crystalline and amorphous lamellae leads to the semicrystalline architecture of starch granules (Zeeman et al. 2010; Compart et al. 2021). Amylose, on the other hand, is essentially linear and amorphous, comprising up to 25% of the granule, and is interspersed within the amylopectin matrix.

Amylopectin content varies between species (Jane et al. 1999; Zeeman et al. 2002). Its branching frequency and chain-length distribution are thought to be the key influences on starch granule morphology. Three types of enzyme activities are involved in amylopectin synthesis. Firstly, SSs (EC 2.4.1.21) transfer the glucosyl moieties from ADP-glucose to existing glucan chains (Nakamura et al. 2005; Fujita et al. 2006; Szydlowski et al. 2009). Secondly, glucan branching enzymes (BEs; EC 2.4.1.18) cleave the α-1,4 bonds of existing glucan chains and attach these to create α-1,6 branching points intermolecularly or intramolecularly (Lu et al. 2015), generating more nonreducing ends available for further glucan elongation. Thirdly, the debranching enzymes (DBEs) limit dextrinase (EC 2.4.1.18) and isoamylases (ISAs; EC 3.2.1.68) are responsible for removing improperly positioned branches, thus promoting crystallization of the amylopectin (Streb et al. 2008; Pfister and Zeeman 2016). Mutants lacking either the BE2 or BE3 homologs show an altered amylopectin structure, with a reduced degree of polymerization (DP) of 5 to 8 glucan chains and increased DP of 8 to 15 glucan chains (Dumez et al. 2006). Moreover, the double mutant *be2be3* is devoid of starch, implying a critical role of these enzymes in starch granule formation (Dumez et al. 2006). Interestingly, the *isa1* mutant, which lacks DBE activity, illustrates the accumulation of soluble phytoglycogen, whose structure is more similar to that of glycogen than that of starch. Compared with starch, it contains increased DP 6 to 8 glucan chains, twice the branching frequency (10%), with the branching points being distributed randomly instead of clustered (Streb et al. 2008). These data demonstrate a clear association between a specific branching pattern and starch crystallization.

Besides the inner structure, starch phosphorylation—the only covalent modification occurring naturally to starch—has been shown to have the capacity to alter starch granule morphology. Starch granule size has been shown to be altered in storage organs of plants when starch phosphate content was changed (Xu et al. 2017; Samodien et al. 2018). The influence of phosphorylation on starch is due to its ability to reduce the starch crystallinity. Using crystalline maltodextrins as the starch model, Hejazi et al. (2008, 2009) demonstrated that phosphorylation facilitated the solubilization of constituent glucan chains. A similar conclusion was also drawn for starch: the introduced hydrophilic phosphate group partially disrupts the double helix structure of amylopectin, converting the highly ordered starch granule surface to a less ordered state that, in consequence, favors the downstream amylolysis (Blennow and Engelsen 2010; Mahlow et al. 2016). The majority of phosphate monoesters are presented at the C6 position and only a small proportion is located at the C3 position of the glucosyl residues within amylopectin (Blennow et al. 1998; Ritte et al. 2006). C6 phosphorylation is exclusively introduced by the GWD (EC 2.7.9.4), whereas C3 phosphorylation is introduced by the phosphoglucan, water dikinase (PWD; EC 2.7.9.5) (Ritte et al. 2004, 2006; Blennow and Engelsen 2010; Hejazi et al. 2014). In vitro and in vivo experiments showed a stronger influence by C6 rather than C3 phosphorylation during starch degradation (Santelia et al. 2011; Hejazi et al. 2012; Mahlow et al. 2016; Malinova, Mahto, et al. 2018).

Phosphate groups are removed from starch by plastidial phosphatases. Two plastidial glucan phosphatases have been identified in plants: starch excess four (SEX4; EC 3.1.3.48) and like sex four2 (LSF2; EC 3.1.3.48) (Kötting et al. 2009; Santelia et al. 2011). SEX4 contributes to the major phosphatase activity and preferentially dephosphorylates at the C6 position of glucosyl residues within amylopectin. However, in vitro analysis shows that it is also capable of dephosphorylating C3 phosphate (Hejazi et al. 2010; Samodien et al. 2018). LSF2 exclusively catalyzes the C3 phosphate release (Comparot-Moss et al. 2010; Santelia et al. 2011). Interestingly, starch granules of the *sex4* mutant show moderate morphological alterations. The starch granules are larger and more spherical than those of the wild type, including some super large granules whose diameters are up to 6 μm (Zeeman et al. 2002; Sokolov et al. 2006). Moreover, *sex4* starch contains a similar phosphate content in the amylopectin fraction but a 4-fold higher amylose content than the wild type, of around 40% (Kötting et al. 2009). The *sex4* mutant reveals an elevated amount of soluble phosphoglucans found to be the result of higher ISA3 and α-amylase3 activities (Kötting et al. 2009). Remarkably, these soluble phosphoglucans were demonstrated to be essentially linear; their content diminished by 30% during the day, leading to speculation about a possible incorporation of soluble phosphoglucans into starch (Kötting et al. 2009). Given the impact of phosphate on the glucan structure, it is tempting to hypothesize that its reduced release by decreased phosphatase activity might interfere with a proper starch metabolism and morphology. Accordingly, it has been demonstrated that the complete glucan hydrolysis via β-amylase3 is impeded by remaining phosphate (Kötting et al. 2009).

The cytosolic DPE2 plays an important role in maltose metabolism: it transfers a glucosyl residue of maltose to cytosolic heteroglycans and releases glucose; its absence results in a significant blocking of maltose consumption (Chia et al. 2004; Dumez et al. 2006). Additionally, an accumulation of soluble oligosaccharides of various lengths was monitored in *dpe2* (Li et al. 2022). Interestingly, the loss of the cytosolic DPE2 also leads to an altered starch granule morphology in

chloroplasts, resulting in rounder and larger starch granules compared with the wild type (Malinova et al. 2017). This result implies an association between altered starch metabolism intermediates and starch granule morphology.

Herein, we found the *Arabidopsis* double mutant *dpe2sex4* showed a bimodal distribution in starch granule diameter, containing 2 types of starch granules, large and small granules, when grown under a light/dark regime. The small granules contained a lower phosphate content on the granule surface, accompanied by higher crystallinity compared with the large granules. We show that starch granule heterogeneity resulted from a discontinued growth of the small granules, which was a potential consequence of their higher crystallinity in which glucan chains were barely elongated during synthesis. These results demonstrate a clear association among starch phosphorylation, starch granule morphology, and size distribution.

Results

Dpe2sex4 shows an unprecedented bimodal starch granule diameter distribution when grown under a 12-h light–12-h dark rhythm, revealing 2 types of starch granules varying in both size and shape

The double mutant *dpe2sex4* was generated by crossing the parent lines *dpe2* and *sex4*. The loss of DPE2 and SEX4 activities was confirmed by native gel and western blot, respectively (Fig. 1A). Phenotypically, *dpe2sex4* had a smaller rosette than the parent lines, with an average of 4-wk-old plant fresh weight of 0.085 g, while *dpe2* and *sex4* had average weights of 0.11 and 0.159 g, respectively. Furthermore, a minor starch turnover was detected with a degradation rate of 5% and 26% lower than *dpe2* and *sex4*, respectively, reflecting degradation deficiency (Fig. 1, B and C). The starch granules of both *sex4* and *dpe2* were larger and more round (lower diameter-to-thickness ratio) compared with Col-0 when analyzed by scanning electron microscopy (SEM). Notably some *sex4* starch granules reached a maximum diameter of up to 9 μm (Fig. 1, D to F). However, the additional loss of DPE2 in the background of *sex4* resulted in the accumulation of 2 types of starch granules—small and large ones. Rather tiny granules with a minimal granule diameter of 0.16 μm accounted for nearly 76% of the total number of granules, whereas the large granules revealed a maximal diameter of 6.97 μm. Thus, the double mutant illustrated a bimodal size, more specifically in terms of diameter, and a distribution of starch granules with 2 peaks at approximate diameters of 0.8 and 4.5 μm. Besides their size, the small granules had a different shape to the large granules, the small granules being spherical and having an average diameter-to-thickness ratio of 1.22, compared with the large granules' ratio of 2.08. The average diameter and thickness of the small granules were 3.6 and 1.1 μm smaller, respectively, than those of the large granules, implying that the small granules were more affected in diameter than in thickness.

A similar bimodal diameter distribution of starch granule was detected and reported in wheat (*Triticum aestivum*) endosperm (Seung and Smith 2019). It was established that small granules in wheat originated from a later starch initiation, along with an anatomical change in the amyloplast (Parker 1985; Langeveld et al. 2000). Starch granule heterogeneous morphology was also reported in the *dpe2phs1* third period, where starch granule number was recovered accompanied by the regeneration of chloroplasts, suggesting a second starch initiation was possibly involved (Li et al. 2022). Different from these 2 mentioned cases, the 2 types of starch granules in *dpe2sex4* coexisted in the same chloroplast and appeared at the same time, i.e. in the first 2 true leaves, which have sprouted less than 2 d (Fig. 1G; Supplementary Fig. S1). Thus, it is more likely that, early on, the double mutant lost control over the homogeneity of starch granule morphology within the same chloroplasts, rather than that a second, time-shifted, starch initiation occurred.

In principle, the presence of the large starch granules in *dpe2sex4* is not surprising given the enhanced blocking of starch breakdown compared with its parent lines. However, the appearance of the small granules was unpredictable. Thus, the question arises of why the small granules exist and to what extent they are different from the large starch granules.

Small starch granules possess a lower phosphate content, less amylose, and a higher degree of crystallinity compared with the large granules

To investigate the different granular characteristics, the 2 types of granules were separated based on their buoyancy in water. The small granules remained in the supernatant, whereas the large granules remained as pellets after vigorous vortexing in distilled water, followed by a settling period of more than 30 min. Using SEM, we validated the purity and confirmed that more than 90% of the small granule fraction had a diameter of less than 2 μm; a similar enrichment was achieved for the large granules (Fig. 2A).

The inner structure of amylopectin, as reflected by the chain-length distribution, revealed that compared with the large starch granules, the small granules had a significantly higher proportion of short glucan chains (DP 4 to 6) and a notably lower proportion of medium glucan chains (DP 18 to 19) and long glucan chains (DP 26 to 32) (Fig. 2B). Thus, the amylopectin was more branched in the small starch granules compared with the large granules, which might be a consequence of the upregulated activity of BEs or downregulated activities of DBEs. Native PAGE and following activity staining revealed that both *dpe2* and *dpe2sex4* showed higher BE2 activity (Supplementary Fig. S2), suggesting that the increased activity in *dpe2sex4* may have been the result of the loss of DPE2. In addition, the small granules contained less amylose, which corresponded with their higher overall crystallinity (Fig. 2C). For analyses of the surface properties, the FTIR spectroscopy ratio at 1,047/1,022 cm^{-1} was analyzed. For small

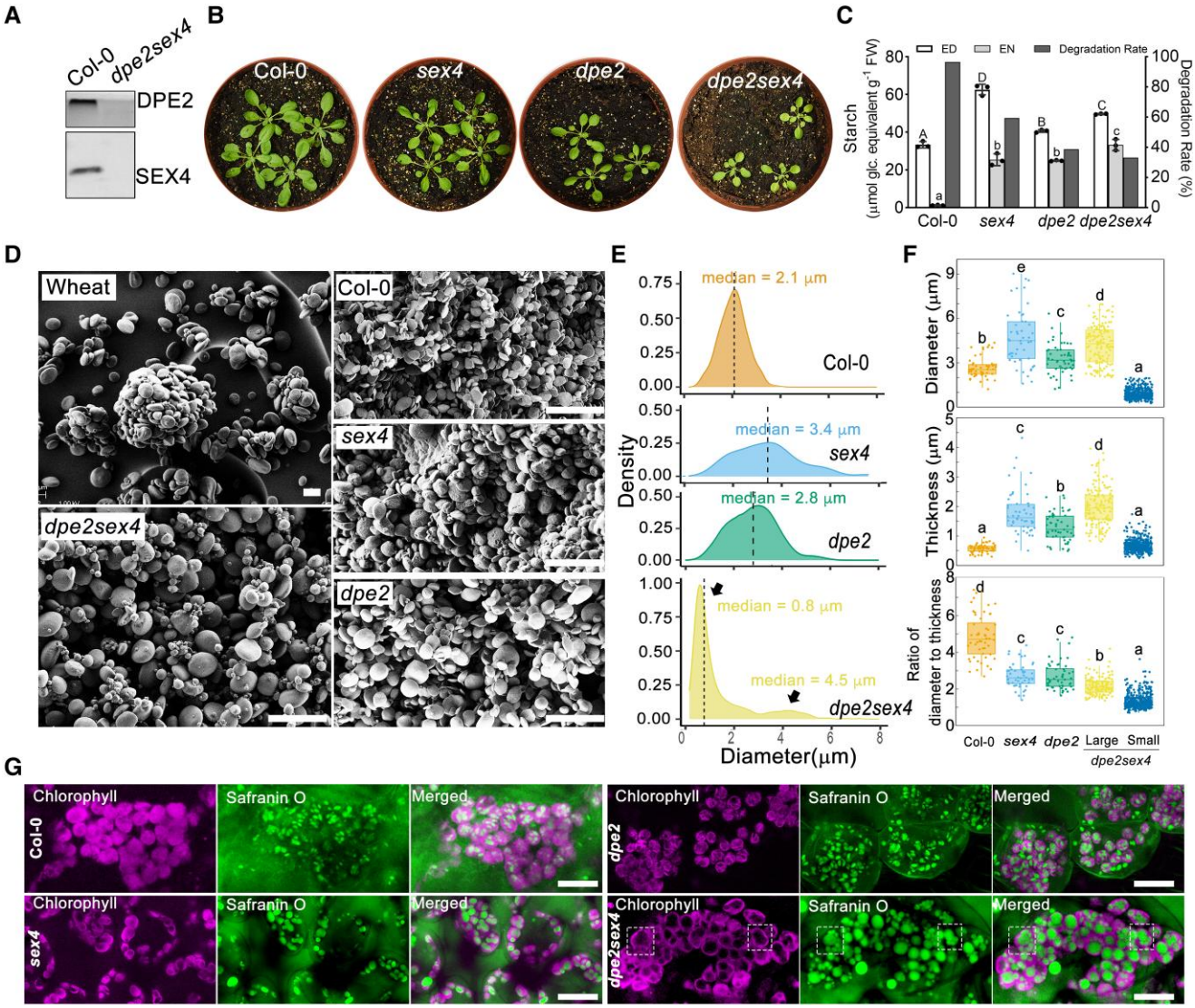

Figure 1. Mutant *dpe2sex4* shows a bimodal distribution in starch granule diameter when grown under 12-h light–12-h dark cycles. **A)** Verification of the inactive DPE2 by native PAGE and detection of SEX4 by western blot. A 10-μg protein was loaded per lane. **B)** Growth phenotype of 4-wk-old plants. **C)** Starch content per fresh weight (FW). The leaves of 4-wk-old plants were harvested, respectively, at the ED and the EN. Mean values and SD are indicated, $n = 3$ independent growth batches. Letters indicate statistically significant differences ($P < 0.05$) based on a 1-way ANOVA followed by Duncan's post hoc test. The third bar of each group represents the rate of degradation (plotted along the *y* axis on the right), derived from averaged values of the starch contents at the ED and EN. **D)** Morphology of starch granules as revealed by SEM. Starch of each line was harvested at the ED. Except for the bar denoting wheat that is 20 μm, all bars equal 10 μm. **E)** Distribution curve of diameters plotted with the median (dotted lines). One milligram of starch was resuspended in 1-mL distilled water, and the starch granules were visualized with light microscopy. More than 10,000 granules were measured to plot each curve. **F)** Starch granule size measurement. Data were collected based on more than 200 granules for large and small types of starch, respectively. Centre line, median; box limits, upper and lower quartiles; whiskers, 1.5× interquartile range; points, individual measurement. Letters indicate statistically significant differences ($P < 0.05$) based on a 1-way ANOVA followed by Duncan's post hoc test. **G)** LCSM analysis of the starch granules in chloroplasts. The dotted boxes indicate the typical coexistence of large and small starch granules in the same chloroplast. All experiments were conducted on 4-wk-old plants, and the leaves were collected at the ED. Bar = 10 μm.

starch granules, a lower FTIR ratio was detected, reflecting a possibly more ordered (and, thus, more closed) surface (Fig. 2C).

A more ordered surface and a higher crystallinity were likely the result of less starch phosphorylation. Thus, we analyzed the phosphate content—the only known covalent modification of starch—in detail. The total phosphate and C6 phosphate content of both types of granules was evaluated using the malachite green kit (Sigma) and a modified enzymatic colorimetric assay (Zhu et al. 2011), respectively. The latter assay uses WST-1 as the oxidant of NADPH to create WST-1 formazan, allowing for an increase in sensitivity

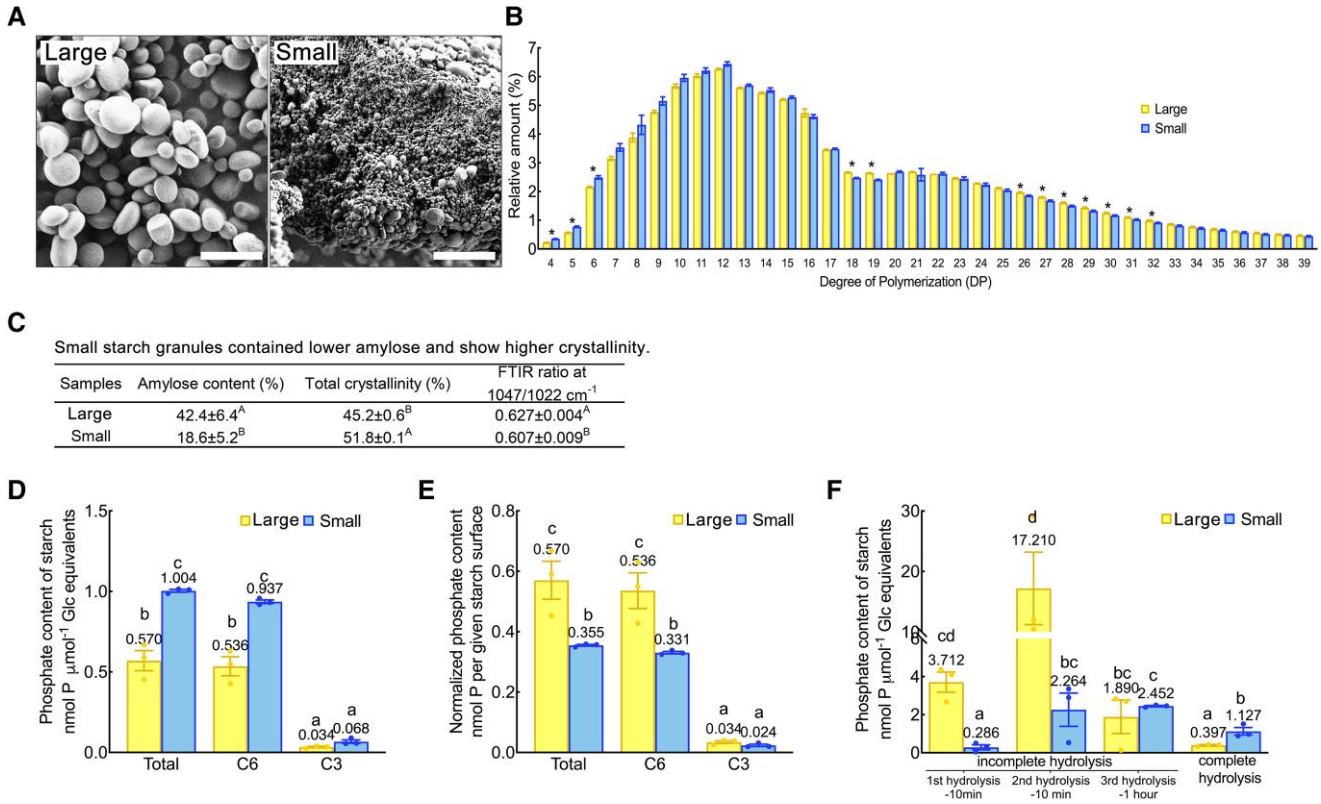

Figure 2. Small granules have a higher phosphate content per glucose equivalents but a lower phosphate content per unit of starch granule surface, a lower amylose percentage, and a higher degree of crystallinity. **A)** SEM confirmation of the segregation of large and small starch granules. Freshly isolated starch from leaf was resuspended in 50 mL of deionized water with a vigorous vortex and held at room temperature for more than 30 min. The small granules were collected from the supernatant, while the large ones were collected from the pellet. The purity was confirmed by SEM. Bar = 10 μm. **B)** Starch chain-length distribution. The released linear glucans were labeled with APTS and detected by capillary electrophoresis equipped with laser-induced fluorescence after ISA digestion of starch. All values are shown with mean ± SD, $n = 3$. Based on a t-test, $P < 0.05$, significant differences between the large and small granules are denoted by asterisks. **C)** Determination of amylose content and crystallinity. To determine the amylose content, 2 mg of starch was dissolved in 1 mL of UDMSO buffer, and the concentration was then determined using the iodine absorption method. $n = 3$; mean values and SD are displayed; letters denote statistically significant differences ($P < 0.05$) based on a t-test. **D)** Quantification of the total phosphate content in the granules per glucose equivalents. Two milligrams of starch harvested at the ED was hydrolyzed with amyloglucosidase and then analyzed with malachite green. All values are shown with mean ± SD, $n = 3$. Letters indicate statistically significant differences ($P < 0.05$) based on a 1-way ANOVA followed by Duncan's post hoc test for **D to F)**. **E)** Normalized phosphate content per unit of starch granule surface. The phosphate content readouts from **D)** were normalized according to Supplementary Fig. S3. In terms of the same weight, the total surface area of small granules was 2.83 times that of large granules. **F)** Localization of phosphate in starch granule. Two milligrams of starch was in turn hydrolyzed partially (without heating) and completely (heating at 95 °C for 10 min) by amyloglucosidase. Alkaline phosphatase liberated the phosphate group, which was then analyzed with malachite green.

and less starch to be used. The starch content in the samples was confirmed enzymatically. The C3 phosphate content was calculated using the total and C6 phosphate values (Fig. 2D).

The total phosphate content was higher in the fraction containing the small starch granules (1.004 nmol phosphate μmol^{-1} glucose equivalents) compared with the fraction containing the large granules (0.57 nmol phosphate μmol^{-1} glucose equivalents). The significant difference in total phosphate content was caused by the C6 phosphate rather than C3 phosphate (Fig. 2D). However, as the small granules differed in their volume-to-surface ratio compared with the large starch granules, we calculated the phosphate content normalized to the starch surface (Fig. 2E). For the same surface area, the small starch granules contained significantly less phosphate than the large starch granules (Fig. 2F; Supplementary Fig. S3).

It has been reported that, in wild type, the starch-phosphate is mainly located at the surface of starch granules (Ritte et al. 2004; Kötting et al. 2009; Mahlow et al. 2014). Thus, we determined the position of starch-phosphate in both starch granule fractions by hydrolyzing them, either completely or partially, and then analyzing the phosphate content with malachite green. In the large granule fraction, most of the phosphate was discovered on the surface; by contrast, for the small granule fraction, the phosphate was detected throughout the granule, with only a minor amount of phosphate on the starch granule surface (Fig. 2F).

Taken together, the small granules revealed a higher proportion of amylopectin that was extensively branched, suggesting that the small granules were more highly organized than the large granules; in addition, the less phosphorylated but higher branched surface implies a more compact granule surface structure. The reduced phosphorylation level on the surface may attribute to the chain-length preference of GWD, as an in vitro experiment revealed that GWD prefers phosphorylating longer glucan chains of DP 30 to 100 (Mikkelsen et al. 2004).

The majority of the starch turnover in *dpe2sex4* occurs on the large granules, as the small granules are inert in starch synthesis

To determine whether the small granules remain unchanged during plant aging, rosettes of *dpe2sex4* were harvested after 2 and 4 wk of growth to evaluate the alteration in starch granule size (Fig. 3, A and B). An increase in the diameter and thickness of large granules was observed. In contrast, no substantial increase in the size of the small granules was detected. Moreover, their proportion of the total granule number remained unchanged, accounting for around 78% of the total starch granules. During the diurnal cycle of 4-wk-old plants, similar to the situation in 2-wk-old plants, a stronger size alteration was detected in large granules. Both the diameter and thickness of large starch granules decreased during the night, although the median change was not statistically significant (Fig. 3B). Most of the starch synthesis, therefore, occurred on the large granules.

The reduced turnover of the small starch granules during the diurnal cycle and its decreased growth rate during leaf aging might be caused by a decreased incorporation of glucose units into the starch granules. This is possibly a consequence of the more compact granule surface structure.

We tested this hypothesis using in vitro incorporation experiments. We used 2 *Arabidopsis* enzymes known to act on the starch granule surface (Fettke et al. 2012; Brust et al. 2014), SS1 (AtSS1; EC 2.4.1.21) and plastidial phosphorylase1 (AtPHS1, EC 2.4.1.1), and ^{14}C-labeled glucosyl donors. In both cases, the ^{14}C-glycosyl residue incorporation in the fraction containing the small starch granules was higher (Fig. 3C). However, when considering the surface area of the granules, the normalized incorporation per unit surface of small granules was still lower than that of large granules, as small granules possessed a surface to volume ratio 2.8 times greater than that of large granules (Fig. 3D; Supplementary Fig. S3). This fact indicates that the morphology of the small starch granules was detrimental to starch synthesis compared with the situation of the large granules.

Starch synthesis is recovered in small granules when the dark phase is omitted

As both SEX4 and DPE2 are involved in nocturnal starch degradation, we germinated and cultivated mutants under continuous light to investigate the influence of the absence of the dark phase on starch granule morphology and size distribution. For *dpe2sex4*, a slightly larger rosette was observed compared with the parent line *dpe2* when grown under continuous light (Fig. 4A), in contrast to the situation observed under light–dark conditions (Fig. 1B). The starch content in *dpe2sex4* (50 mmol glucose equivalent per gram fresh weight) was between that of both parental lines (60 and 41 mmol glucose equivalent per gram fresh weight in *sex4* and *dpe2*, respectively; Fig. 4B). Moreover, starch granule morphology was affected, as it was homogeneously discoid and exhibited a unimodal size distribution, whose diameter median was around 4 μm, similar to those of the parent lines (Fig. 4, C and D). Thus, no variation in starch granule morphology was observed within *dpe2sex4* upon the omission of the dark phase. The result was confirmed by laser confocal scanning microscopy (LCSM) analysis (Fig. 4E).

One possible hypothesis is that the small granules synthesized under the diurnal light cycle resulted from disordered situation/structures (e.g. disordered nucleation of high phosphorylated and improper branching oligosaccharides) at the beginning of granule formation when the dark phase was presented, and the lack of the dark phase would stop this process. This would mean that a later lack of the dark phase would not have such consequences and the bimodal morphology would remain. To investigate this possibility, we transferred 2-wk-old plants grown under the light–dark regime to continuous light conditions. Plants were exposed to continuous light for only 5 d to prevent the formation of new leaves. The diameter of the small granules of *dpe2sex4* was almost twice as large as it was before the transition (Fig. 5, A and B), whereas there was no discernible size increase observed even after 2 wk when grown under light–dark conditions (Fig. 3). Thus, the further synthesis of the small granules without the dark phase during a later time of growth, when the starch granules were already initiated, excluded the possibility that a disordered situation during the beginning formation of the granules was responsible for the different starch granule types. In contrast, it shows that the lack of the dark phase, independent of leaf development, results in a reuse of the small starch granules for starch synthesis. Further, it also shows that the compact granule surface structure observed in the case of small granules can be overcome for further starch synthesis.

In all 4 genotypes, a substantial increase in the diameter rather than the thickness was observed (Fig. 5, B to D). In terms of the relative growth in diameter, the large granules increased by 129%, which was comparable to the situation in the parental lines. In contrast, the small starch granules of *dpe2sex4* increased by 285%, which was the strongest alteration observed.

dpe2sex4 accumulates a large number of soluble highly branched phosphorylated glucans when grown under light/dark conditions, whereas the amount is decreased under continuous illumination. As mentioned, the C6 phosphorylation of starch was primarily responsible for the difference in starch-phosphate content between the large and small starch granules and, hence, thought to be at least partially

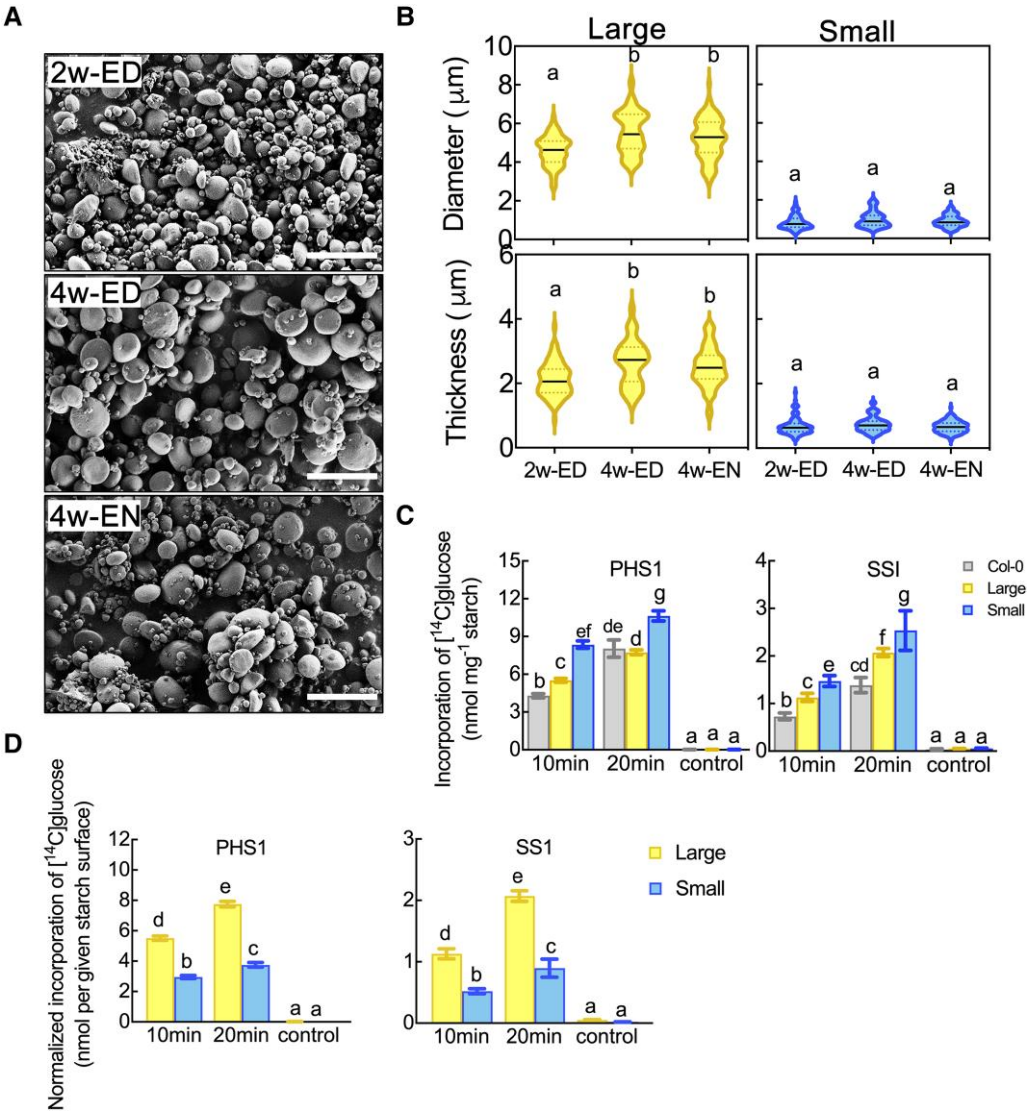

Figure 3. Small starch granules are inert in starch synthesis. **A)** SEM analysis of *dpe2sex4* starch granules collected at the indicated times. Bar = 10 μm. **B)** Size comparison of large and small starch granules harvested at various time points. For measuring each type of starch, more than 200 granules were utilized. **C)** Incorporation of glucosyl residues by SSI or PHS1 into native starch granules. Five milligrams of each type of starch granules was incubated at 30 °C for 5 and 10 min with 0.1 μg of AtSS1 or AtPHS1 under constant shaking. The reactions were terminated with 2% (w/v) SDS, and the samples were thoroughly washed 3 times with water before [^{14}C]glucosyl residue incorporation was determined using scintillation counting. Inactive SS1 or PHS1 was used as the control, respectively. **D)** Normalized incorporation of glycosyl residues considering the effect of starch granule surface. The values are mean ± SD ($n = 3$). Letters denote statistical significance as determined by ANOVA and Tukey's post hoc test ($P < 0.05$) for **B to D)**.

responsible for the generation of these 2 types of starch granules in *dpe2sex4*. We therefore also analyzed starch phosphorylation under continuous light, when a monomodal starch granule size distribution was detected (Fig. 4).

dpe2sex4 starch possessed less C6 phosphate than those of its parent lines at the end of the day (ED) but a similar amount of phosphate as *dpe2* starch at the end of the night (EN). Small granules of *dpe2sex4* revealed no alteration in C6 phosphate content when ED and EN were compared. The starch from 3 lines, Col-0, *sex4*, and *dpe2*, all contained less C6 phosphate at EN than at ED (Fig. 6A). The exception observed in *dpe2sex4* is likely the result of the uneven starch metabolism of large and small granules. Since starch turnover primarily occurred on the large starch granules (Fig. 3), in contrast, no obvious size alteration of small granules between ED and EN was detected; thus, at EN, the mass proportion of small granules increased (although its proportion of the total granule number remained unchanged, accounting for around 76% of the total starch granules). In addition, small granules contained higher C6 phosphate amount than large granules at both ED and EN; thus, a higher phosphate amount was observed at EN in *dpe2sex4*.

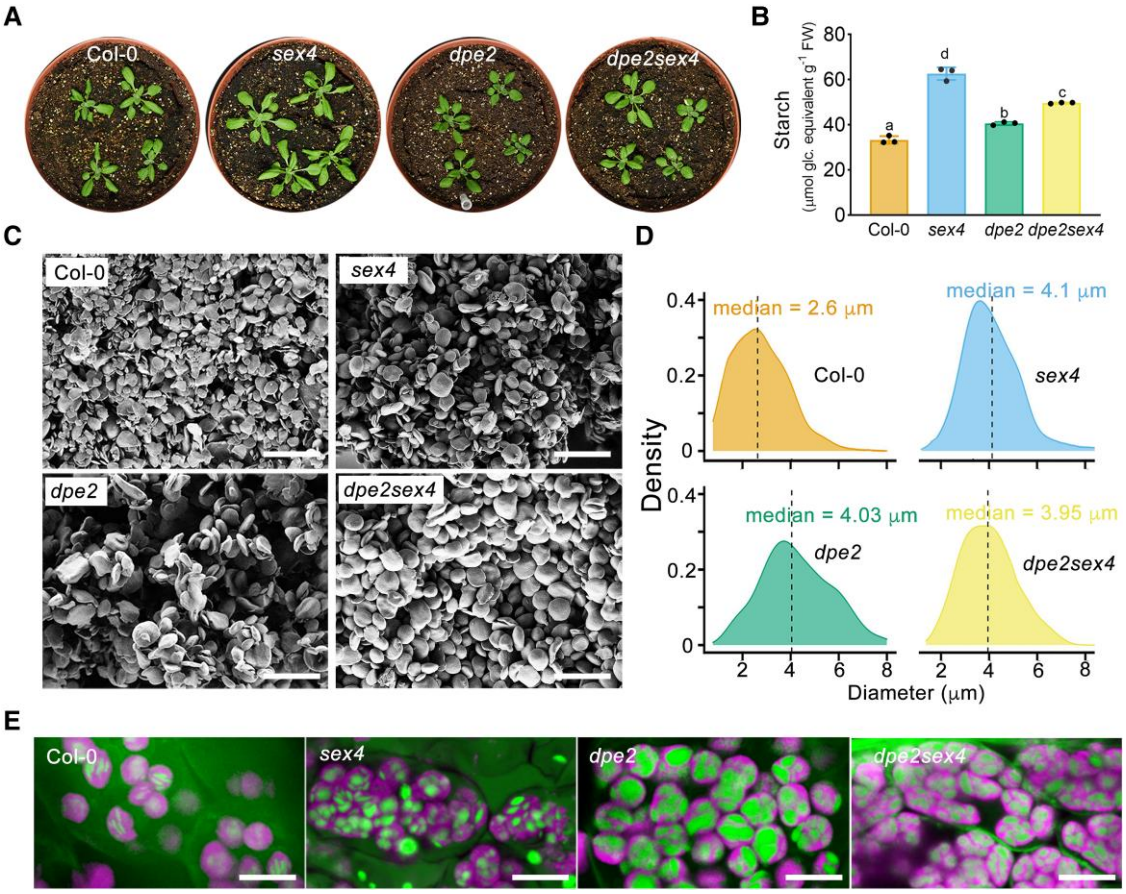

Figure 4. Mutant *dpe2sex4* shows a unimodal starch granule diameter distribution when germinated and cultivated under continuous light. All leaf materials used here were harvested from plants that were 2.5 wk old. **A)** The rate of the plant growth phenotype. **B)** Quantification of the starch content per fresh weight (FW). The values are mean ± SD ($n = 3$). Letters denote statistical significance as determined by ANOVA and Tukey's post hoc test ($P < 0.05$). **C)** The morphology of starch granules as revealed by SEM. Bar = 10 μm. **D)** Diameter distribution curve plotted with the median (dotted lines). One milligram of starch was resuspended in 1 mL of distilled water, and the starch granules were observed under a light microscope. For each curve, more than 10,000 granules were measured. **E)** Diagnosis of starch granules in the chloroplast with LCSM. Bar = 10 μm.

In terms of growth conditions, and comparing starch phosphate content, we found that the highest phosphate content of Col-0 was detected under continuous light, and it was nearly twice as high as that at ED, similar to a previous result (Hejazi et al. 2014). In *dpe2sex4*, the highest C6 phosphate content of starch was also measured under continuous light. However, in *dpe2* and *sex4*, the lowest C6 phosphate content of starch was discovered under continuous light.

For *sex4*, it was found that linear phosphorylated soluble glucans were accumulated (Kötting et al. 2009). We therefore also analyzed the soluble glucans in the 4 genotypes. When grown under light/dark conditions, *dpe2sex4* accumulated more soluble glucans than Col-0 and *sex4* but similar amounts to *dpe2* (Fig. 6B). However, when grown under continuous light, the smallest amount of soluble glucan was detected in *dpe2sex4*. The degree of branching was rather similar in all genotypes, independent of the growth conditions (Fig. 6C). At all 3 time points, the soluble glucans in *dpe2sex4* had the highest degree of branching among the 4 genotypes, with a peak at ED.

Nevertheless, in contrast to the starch situation where *dpe2sex4* contained the lower C6 phosphate content than the parent lines under diurnal conditions but a higher amount under continuous light, in the soluble glucans, the C6 content was the highest in *dpe2sex4* under light/dark conditions but the lowest under continuous light among all genotypes (Fig. 6D). Thus, *dpe2sex4* had a large quantity (Fig. 6B) of highly branched (Fig. 6C) and phosphorylated (Fig. 6D) soluble glucans when grown under the light/dark rhythm. These soluble glucans were not accumulated under continuous light (Fig. 6B); moreover, they displayed less phosphorylation (Fig. 6D). After ISA treatment, we found that the predominant length of the branched chains of the soluble glucans in *dpe2sex4* revealed a DP of 2 (Supplementary Fig. S4).

Discussion

Several starch-related genes that somehow influence starch granule size, shape, or morphology have already been

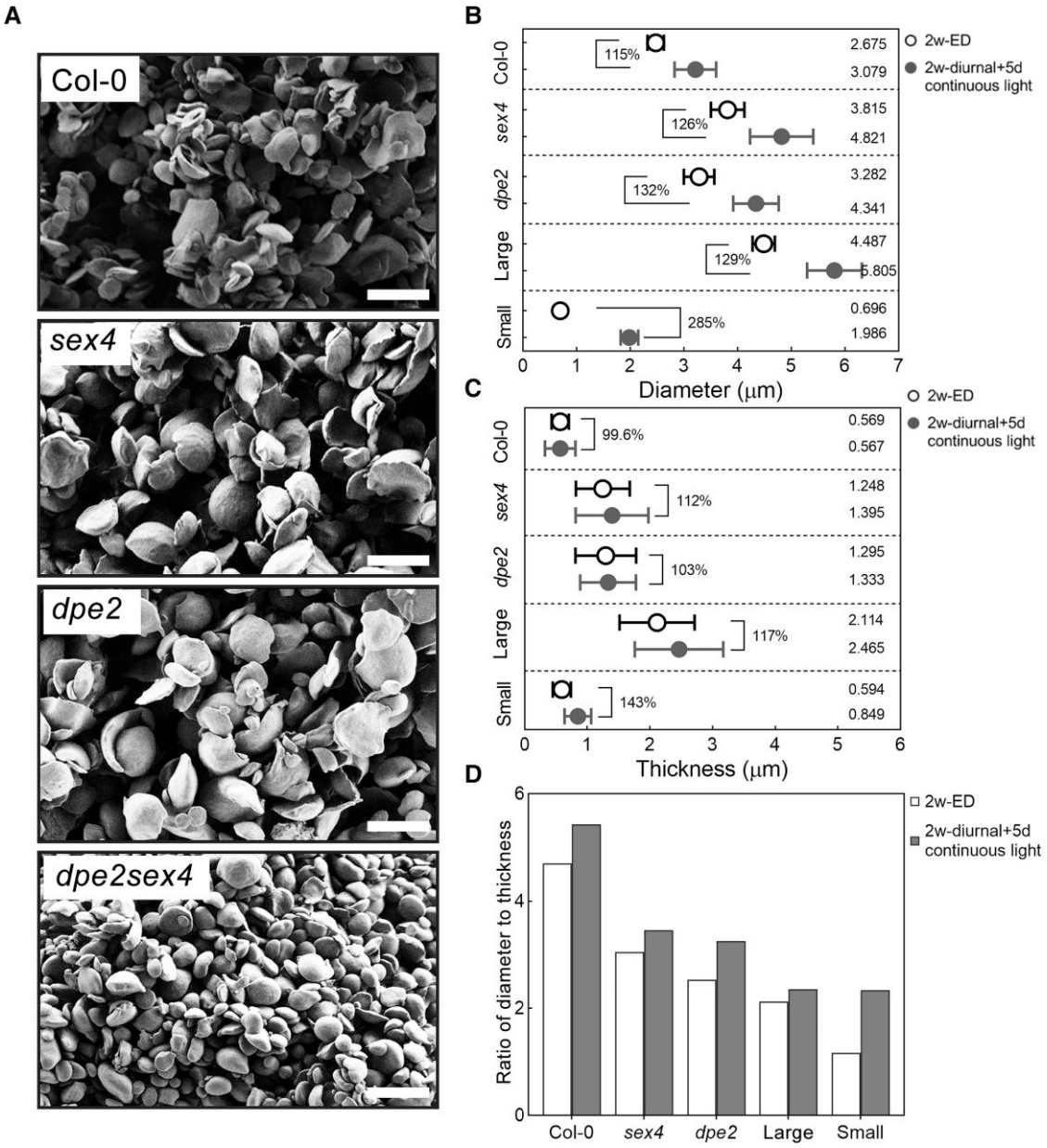

Figure 5. The recovery of starch synthesis in small granules by a delayed omitting of the dark phase. All plants were grown under 12-h light–12-h dark conditions for a period of 2 wk, after which half of the plants from each line were harvested at the ED (2w-ED); the remaining plants were transferred to continuous light for 5 d (2w-diurnal + 5 d continuous light). **A)** The starch granule morphology of the plants transferred to continuous light. Bar = 10 μm. **B, C)** The measurement of starch granule diameter and thickness, after the plants were transferred to continuous light. Mean values (numbers on the right) and 95% CIs are presented (nonoverlapping intervals represent significant differences); the calculation was based on more than 200 granules of each line. The percentage depicts the size alteration rate. **D)** The ratio of diameter to thickness after transition, plotted according to the mean values of diameter and thickness, respectively.

described (Seung and Smith 2019; Liu et al. 2021; Mérida and Fettke 2021). The molecular mechanisms that affect these parameters are still obscure; however, all the described single, double, and triple mutants revealed homogeneous starch granules. Thus, all starch granules of mesophyll cells become more spherical, as in the case of *ss4* or *dpe2* (Liu et al. 2021), or more uneven but still discoid, as in the case of *gwd* (Malinova and Fettke 2017). So far, nonhomogeneous (bimodal or polymodal) starch granule size distributions in mesophyll cells of *Arabidopsis* have never been reported.

The unique starch metabolism in *dpe2sex4*

The *dpe2sex4* double mutant revealed an unprecedented starch granule phenotype. We observed small (mean of 0.8 μm) and large granules (mean at 4.5 μm) within the same chloroplast (Fig. 1), the mean size difference being

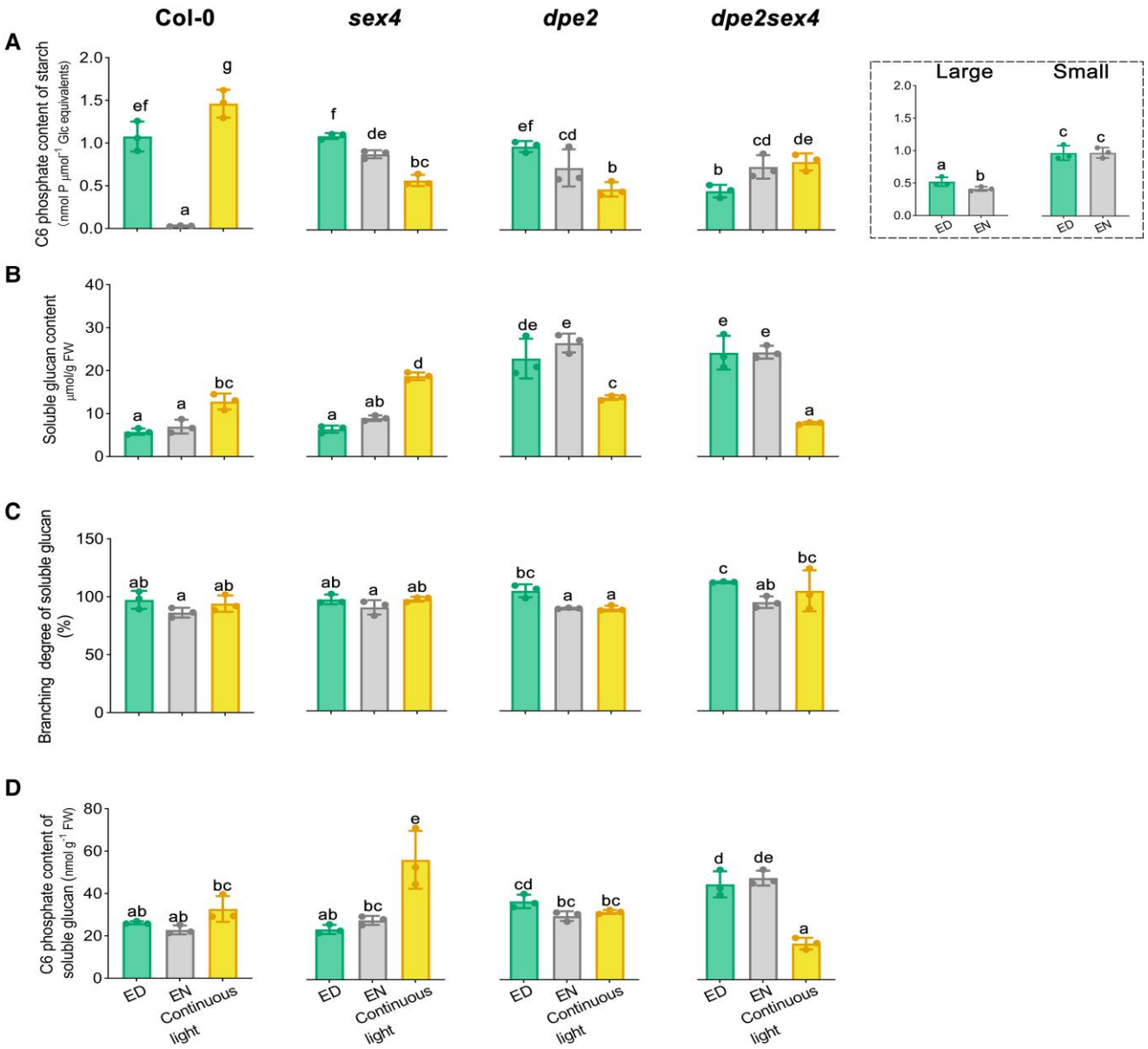

Figure 6. C6 phosphate content analysis in starch and corresponding soluble glucan. The measurement was based on a colorimetric enzymatic method with WST-1 reagent (Sigma) (Zhu et al. 2011). **A)** Determination of C6 phosphate content in starch isolated from ED, EN, and continuous light. Two milligrams of starch of each line was used and hydrolyzed by amyloglucosidase. The liberation of phosphate groups was performed with alkaline phosphatase (AP). The values are mean ± SD ($n = 3$). Letters denote statistical significance as determined by ANOVA and Duncan's post hoc test ($P < 0.05$) for all the graphs in this figure. **B)** Determination of soluble glucan content; 50 to 100 mg of leaf materials were harvested and extracted according to Kötting et al. (2009). Measurement of reducing sugars was conducted to indicate the amount of soluble glucan. **C)** Branching degree analysis of soluble glucan. Soluble glucans were extracted from 50-mg leaves as described (Kötting et al. 2009), after measurement of reducing sugars with a BCA assay using cupric ion as an oxidant (Doner and Irwin 1992), 100 nmol of soluble glucans were withdrawn and subjected to ISA treatment for 1 h, and the amount of soluble glucan was measured again (Doner and Irwin 1992). **D)** Determination of the C6 phosphate content of soluble glucan; 50 to 100 mg of leaf materials were harvested and extracted according to Kötting et al. (2009). After amyloglucosidase digestion and phosphate liberation by AP, the phosphate content was measured.

more than 5-fold. A comparable situation is, however, described in endosperm storage starch of temperate cereals like wheat (Parker 1985; Langeveld et al. 2000). Similar to the situation for *dpe2sex4*, 2 different starch granule types were detected within the same amyloplast, termed as A-type and B-type granules. The size of the larger A-type granules was approximately 20 to 30 μm and that of the smaller B-type granules was around 2 to 7 μm. Thus, the size difference was around 4- to 8-fold. In addition, it was shown that, in wheat, the initiation of A-type granules occurred at the onset of endosperm development, whereas the B-type granules initiated at least 10 d later

(Bechtel et al. 1990). Further, the location of the different starch granule types was different, with the A-type initiated in the amyloplast, whereas the B-type granules were located in small excrescent stromules of the amyloplast (Langeveld et al. 2000). Thus, it is highly likely that different proteins/enzymes or carbohydrate primer molecules are involved in the starch granule initiation as the biosynthetic processes for the 2 granule populations were found to be separate, both spatially and in time. It is worth mentioning that this phenotype of bimodal starch granule size distribution in wheat is organ specific and the mechanisms are likely to be different from *Arabidopsis* transient starch (Chen et al. 2022). Moreover, endosperm starch in wheat is synthesized in amyloplasts whereas leaf starch in *Arabidopsis* is synthesized in chloroplasts, with stromal pockets as a defined space of starch granule initiation, potentially influencing starch granule synthesis and morphology as well (Bürgy et al. 2021; Esch et al. 2022). This was not the case in *dpe2sex4*, as the granules were found within the same chloroplast and no indication of a spatial separation was found (Fig. 1). Similarly, we show that both types of starch granules were detectable in the first true leaves (Supplementary Fig. S1), which is very early, and at the same developmental stage. Therefore, it is more likely that both types of granules were initiated by the same molecular mechanism but then metabolized differently. This assumption was confirmed by several independent experiments. We demonstrated that the properties of starch granules differed (see below). Further, we showed that, in the total absence of a dark phase during growth, starch granule size distribution changed to be homogenous, in that it is more similar to the situation of the larger granule fraction (Fig. 4). Even a short continuous light phase after a 2-wk-long light/dark phase of growth revealed a tendency that both small and the large starch granule types became more similar (Fig. 5), with the smaller granules increasing in both diameter and thickness. Our in vitro experiments showed that the small and large granule fractions were differently used by starch-synthesizing enzymes. Two enzymes, SS1 (a major SS activity detectable in *Arabidopsis* leaves; Brust et al. 2014) and plastidial phosphorylase (capable of incorporating glucosyl residues into native starch granules depending on the granule surface structure; Fettke et al. 2012; Mahlow et al. 2014), were used. For both enzymes, differential utilization of the 2 starch granule types was detected with a much better incorporation of glucosyl residues into the large granules. Taking all this together, we show that the large starch granules display a more intensive turnover than the smaller granules under normal growth conditions. However, this is not fixed, implying that not only is the existing starch granule structure responsible, but that metabolites or metabolic processes are also involved.

Interestingly, when growing *dpe2sex4* under normal light/dark conditions, often only 1 large starch granule per chloroplast was found, accompanied by several small granules, but we rarely detected more than 2 large starch granules per chloroplast. The total granule number per chloroplast was typical as normally observed in wild type. Of 168 analyzed chloroplasts, 139 possessed 1 large granule accompanied with several small granules. In 19 chloroplasts, 2 large granules were detected (Supplementary Fig. S5). A similar situation also occurs in other *Arabidopsis* single and double mutants, e.g. *ss4* or *dpe2phs1* (in the reduced granule period, where the starch granule number in young leaves reduces from normal level to one), and in *ptst2* (Seung et al. 2017; Li et al. 2022). As already speculated, one possible explanation for this effect is that, normally, 1 granule is initiated by a primal initiation process and all further starch granules in the chloroplast are initiated as a result of further involved proteins and enzymes (Malinova, Qasim, et al. 2018; Mérida and Fettke 2021). Thus, in various mutants, only the additional granules are affected but not the primal-initiated granules. Following this idea, a metabolite is, again, expected to affect the formation of several small granules. Accordingly, *dpe2sex4* displayed the typical expected number of starch granules per chloroplast as in wild type. However, as the granules were very tiny, an underestimation of this number is, in principle, possible.

Characteristics of the small starch granules in *dpe2sex4*

We lack any observation of spatial and time separation for either type of starch granule in *dpe2sex4*. However, understanding the structural differences between both granule types that somehow account for different usage during starch turnover is, of course, of critical importance. We showed that the smaller starch granules displayed an altered inner structure, with a higher degree of branching, less phosphate, less amylose content, and a more closed surface structure (Fig. 2). As neither the *dpe2* nor *sex4* single mutant displayed a nonhomogeneous starch granule size distribution, but both single mutants displayed a starch excess phenotype, a mechanism simply based on reduced starch degradation is not an explanation. Similarly, even a total starch degradation block, such as in *sex1-8* (GWD mutant; Mahlow et al. 2014; Malinova and Fettke 2017), or strongly inhibited starch degradation, such as in *pwd* or *bam3* mutants (Mérida and Fettke 2021), did not result in nonhomogeneous starch granules. It is more likely that the lack of C6 phosphate utilization by the starch, directly or indirectly, affected the starch granule size distribution (see below). It was already shown that starch phosphorylation is also important during starch synthesis (Hejazi et al. 2014). Interestingly, the phosphate inside the starch granules was found differently distributed in the 2 types of starch granules (Fig. 2, D to F). In the small granules, C6 phosphate was distributed within the entire granule (Fig. 2F), whereas in most cases, although never exclusively, C6 phosphorylation was mainly reported at the starch granule surface (Hejazi et al. 2012). The data, to some extent, may underestimate the difference in distribution, as the small granules are more crystalline and display a more closed surface structure compared with the large starch granules. Thus, a partially randomly acidic hydrolysis is more likely to act on less compact structures. However, as the phosphate content was determined per released glucose,

it clearly reveals that, in the case of the small starch granule fraction, the phosphate is deeply trapped inside the granules.

As the small granules can be reused during starch synthesis under continuous light (Fig. 5), starch phosphorylation cannot be the only factor regulating size distribution. It is more likely that, during starch degradation (or related to the dark phase), another metabolite is responsible for the nonhomogeneous distribution.

Interestingly, when the small starch granules were reused during starch synthesis, i.e. during continuous light (Fig. 5), the major changes in morphology were related to the increase in starch granule diameter and to a lesser extent to the increase in thickness. Unfortunately, the molecular mechanism behind this is still largely unknown.

The molecular mechanism behind the nonhomogeneous starch granule size distribution

As previously mentioned, small starch granules can be reused for starch turnover under continuous light. Hence, a metabolic control is likely. A strong difference was observed in the presence of soluble glucans. Thus, under continuous light, when starch granule distribution became homogenous, there were far fewer soluble glucans, and the still-detectable glucans were much less phosphorylated. In no other genotype, such high levels of soluble branched phosphoglucans have been detected (Fig. 6). Thus, there is supposedly a link with the observed starch granule phenotype. Furthermore, other metabolites are assumed to have an effect on starch morphology; indeed, the accumulation of maltose seems to result in more spherical starch granules (Malinova et al. 2017; Li et al. 2022).

The highly phosphorylated soluble glucans were obviously not used for further starch granule initiation. Of interest, however, is the turnover of this soluble glucan pool, which is probably low, as phosphorylation prevents total degradation by hydrolytic enzymes.

This work clearly shows a bimodal distribution of starch granule size in *dpe2sex4*, an unprecedented phenotype in transitory starch. These data provide valuable insights into the previously understudied aspect of starch granule morphological homogeneity, specifically the involvement of starch phosphorylation and degradation metabolites. Further studies, such as into the molecular mechanism underlying the formation of small granules and the effect of varying lengths of the dark phase, will be helpful to understand starch granule morphological homogeneity in detail. Given the impact of phosphorylation on starch modification, small granule characteristics, such as gelatinization, retrogradation, and digestibility, are necessary to enable the broadening of industrial applications.

Materials and methods

Plant materials and growth conditions

To generate the *A. thaliana* knockout line *dpe2sex4*, *dpe2-5* (SALK_073273C; Chia et al. 2004) was crossed with *sex4-3* (SALK_102567; Niittylä et al. 2006) and self-pollinated the F1 generation. The activity of DPE2 was monitored by native gel and zymogram techniques, as described by Fettke et al. (2005). Western blot analysis was conducted to confirm the absence of SEX4 protein, following the protocol (Niittylä et al. 2006).

Sterilized seeds were sown on MS medium containing 0.8% (w/v) agar, pH 5.7, and then vernalized in darkness at 4 °C for 3 d. After 5 to 7 d, the seedlings were transplanted to the soil. The plants were grown under 3 different conditions: a light/dark regime (12-h light, 20 °C, 110 μmol m^{-2} s^{-1}; 12-h dark, 16 °C; 60% relative humidity), continuous light (20 °C, 110 μmol m^{-2} s^{-1}; 60% relative humidity), or a combination of the two.

SEM and starch granule diameter distribution curve plotting

The isolation of native starch granules and SEM analysis were performed as described elsewhere (Malinova et al. 2017). To plot the diameter distribution curve, a suspension of 1-mg starch in 1-mL distilled water was prepared, which was then observed under a light microscope. More than 10,000 starch granules were measured using the ImageJ software.

LCSM

Harvested leaves were immersed in a safranin O solution (5 g/L) for 20 min. The starch and chlorophyll signals were visualized using a Zeiss LSM 880 Airyscan confocal microscope with a 63× oil-immersion lens with a 1.4 numerical aperture. Safranin O signals and auto-fluorescence of chlorophyll were monitored using an argon laser at a 488-nm wavelength for excitation, and the absorption peaks were from 510 to 690 nm and from 640 to 696 nm, respectively (Liu et al. 2021).

Estimation of total phosphate and C6 phosphate content of starch

Total phosphate content was measured using the malachite green kit (Sigma). Two mg of starch was washed 3 times with distilled water and then gelatinized by heating at 95 °C for 10 min. The solubilized starch was hydrolyzed by 1 U of amyloglucosidase (Roche) in 100-μL water at 25 °C for 2 h. A 50-μL aliquot of the resulting sample was incubated with 15 U of alkaline phosphatase (Thermo Fisher) for 2 h at 37 °C in a final volume of 100 μL. Reaction termination and protein elimination were conducted by heating the solution at 95 °C for 10 min. After centrifugation at 4 °C, 17,000 × *g* for 10 min, an aliquot of the resulting solution was taken to determine the released orthophosphate using the malachite green reagent according to the manufacturer's protocol. The absorbance at 660 nm was read by a Tecan microplate reader. A standard curve was also prepared using the kit. All assays were performed in triplicate.

C6 phosphate content was quantified by an adapted enzymatic colorimetric method using WST-1 reagent (Sigma),

based on Zhu et al. (2011). Two milligrams of starch was solubilized and completely hydrolyzed with amyloglucosidase, as above. After the elimination of protein contamination and centrifugation, the subsequent supernatant was dried in a speed vacuum centrifuge (Thermo Savant SPD111V-115) and then resuspended in 100 μL of 50 mM Tris buffer (pH 8.5). Each reaction mixture contained 80-μL aliquot of the sample and 20-μL assay solution. The assay solution was prepared by mixing the following: 5 μL of 20 mM $MgCl_2$, 0.5 μL of 5 mM $NADP^+$, 5 μL of WST-1, 5 μL of 0.1 mM PMS, 0.1 U of G6PDH (Sigma), and 50 mM Tris buffer (pH 8.5) to a final volume of 20 μL. The reaction was incubated for 2 h in the dark at room temperature. The absorbance was measured at 440 nm with a microplate reader. Serially diluted G6P standards treated the same way were used to generate the standard curve.

Starch content quantification

The starch content (glucose equivalents) was quantified via 2 methods. For the phosphate content of starch, the same enzymatic colorimetric method using WST-1 reagent was performed. In addition to the components mentioned above, 5 μL of 11 mM ATP and 0.1 U of hexokinase (Sigma) were also included in the assay solution, and the sample was diluted accordingly. A glucose standard was similarly prepared and utilized in the assay.

Leaf starch content was determined according to Fettke et al. (2011).

Detection of the phosphate localization

The granules were hydrolyzed either completely or incompletely. Without disrupting their natural structure, 2 mg of native granules was incubated with 1 U of amyloglucosidase at 25 °C for varying durations, as indicated, allowing the glucose to be released layer by layer. After 3 rounds of incomplete hydrolysis, the remaining starch was heated at 95 °C for 10 min and then completely hydrolyzed by amyloglucosidase. The released phosphate was quantified using a malachite green reagent as described above.

Measurement of C6 phosphate content and the branching degree of the soluble glucans

The soluble glucans were extracted as described (Kötting et al. 2009). Liquid nitrogen-frozen leaves (50 mg) were homogenized using a motor and a grinder sequentially. An amount of 500 μL of cold 1 M perchloric acid was added to the sample, which was then vigorously mixed. After 15 min of centrifugation at 4 °C and 3,000 × *g*, the supernatant was adjusted to a pH of 5.0 by 2 M KOH, 0.4 M MES, and 0.4 M KCl. After a second centrifugation (20,000 × *g*, 15 min, 4 °C), the supernatant was collected and concentrated in a speed vacuum centrifuge.

Using the same enzymatic colorimetric method (Zhu et al. 2011), the C6 phosphate content of soluble glucan was determined. Firstly, the soluble glucan was hydrolyzed for 2 h at 40 °C with 1 U of amyloglucosidase. After removing the protein by heating at 95 °C for 10 min, the resulting solution was evaporated and resuspended in 100 μL of 50 mM Tris buffer (pH 8.5). As stated previously, a total volume of 100 μL was used for each reaction, which included a 20- to 80-μL aliquot of the sample solution.

The branching degree of soluble glucan was quantified by the content difference of the reducing ends after ISA (Megazyme) treatment. A quantity of 100 nmol of soluble glucan was treated with 1 U of ISA at 40 °C for 1 h with constant agitation, followed by the measurement of reducing ends with a Bicinchoninic Acid (BCA) Method assay using cupric ion as oxidant (Doner and Irwin 1992).

Chain-length distribution analysis of starch and maltodextrin

Five milligrams of starch was solubilized by heating at 99 °C for 10 min and then hydrolyzed by 2 U ISA overnight at 40 °C. The released glucans were collected, 100 nmol of which was labeled using 8-aminopyrene-1,3,6-trisulfonic acid, trisodium salt (APTS). Chain-length distribution was analyzed by capillary electrophoresis equipped with laser-induced fluorescence detection (CE-LIF) (Malinova and Fettke 2017).

The soluble glucan was extracted as described above; after the measurement of reducing ends, 100 nmol of soluble glucan was labeled with APTS and analyzed using CE-LIF.

Amylose content

The apparent amylose content was determined using an iodine absorption method (Konik-Rose et al. 2007). In summary, 2 mg of starch was dissolved in 1 mL of UDMSO solution (9 parts DMSO and 1 part 6 M urea) by heating at 95 °C for 1 h under constant shaking. The reaction mixture in a total volume of 1 mL included 50-μL aliquot of dissolved starch sample, 20 μL of iodine solution (2 mg iodine and 20 mg potassium iodide per mL of water), and water. The absorbance was measured at 620 nm. A standard curve was generated using a series of amylose standards (Sigma, potato tuber starch) ranging from 0% to 90%.

Zymograms of hydrolytic activities

Hydrolytic activities (BEs, ISAs, and BAMs) were analyzed by native PAGE and zymograms as described (Wattebled et al. 2005). One hundred micrograms of leaf-soluble proteins were separated with a polyacrylamide gel (7.5% v/v) containing 0.3% (w/v) soluble potato starch (Sigma). After migration under native conditions, gels were incubated overnight in the following buffer: 50 mM trisodium citrate, pH 6.0, 50 mM Na_2HPO_4, and 5 mM DTT. Enzyme activities were visualized by iodine staining.

Quantification of incorporation of [^{14}C]glucosyl residues

SS1 mediated glucosyl residues incorporation

The reaction mixture contained 10 mg of starch granules, 0.1 μg of AtSSI, 1 mM ADP-glucose, 0.08 μCi [glucosyl-^{14}C]

ADP-glucose, 200 mM Na-citrate, 0.025% (w/v) BSA, and 10 mM tricine/NaOH (pH 8.0). The samples were shaken constantly while incubated at 30 °C. The reactions were stopped at 10- and 20-min intervals with 2% (w/v) SDS. After washing the starch granules 3 times with water, the incorporation of [^{14}C]glucosyl residues was assessed using scintillation counting.

PHS1 mediated glucosyl residues incorporation
The reaction mixture contained 10 mg of starch granules, 200 mM Na-citrate (pH 6.5), 1 mM glucose-1-phosphate, 0.5 μCi [U-^{14}C]Glc-1-P, and 0.1 μg of PHS1. The reaction was incubated at 37 °C under continuous agitation for the 2 time periods noted above. The reactions were stopped as described above, and the incorporation of ^{14}C was determined.

Total relative crystallinity analyzed by the wide-angle X-ray scattering

The crystalline structure of starch granules was evaluated by a Nano-inXider instrument (Xenocs SAS, Grenoble, France), equipped with a Cu Kα source with a 1.54-Å wavelength and a 2-detector setup (Zhong et al. 2021). Briefly, starch samples equilibrated at ~80% relative humidity were sealed in 5- to 7-μm mica films. The radially averaged intensity I was given as a function of the scattering angle 2θ in the angular range of 5° to 35°. The total relative crystallinity was calculated as the ratio of the crystalline peak area to the total diffraction area using PeakFit software (Version 4.0, Systat Software Inc., San Jose, CA, USA).

Short-range ordered surface structure variation analyzed by FTIR spectroscopy

The ordered structure of the starch granule peripheral parts was analyzed using a Bomem MB100 FTIR instrument (ABB-Bomem, Quebec, Canada) according to the method described by (Zhong et al. 2021). The instrument was equipped with an attenuated total reflectance single reflectance cell with a diamond crystal. The starch samples were scanned 64 times over the range of 4,000 to 600 cm^{-1} at a resolution of 8 cm^{-1} against air. Spectra were calibrated by a baseline in the region from 1,200 to 800 cm^{-1} and were deconvoluted using OMNIC 8.0. The line shape underlying distributions were assumed to be Lorentzian with a half-width of 19 cm^{-1}, and a resolution enhancement factor of 1.9 was used. The ratios of absorbances at 1,047/1,022 cm^{-1} were obtained to estimate the short-range ordered structure of starch granule.

Statistical analyses

One-way ANOVA followed by Tukey's or Duncan's multiple comparisons test and Student's *t*-test analyses were used to determine statistically significant differences.

Accession numbers

Sequence data from this article can be found under the following accession numbers: SEX4 (At3g52180), DPE2 (At2g40840), PHS1 (At3g29320), SS4 (At4g18240), SS1 (At5g24300), GWD (At1g10760), LSF2 (At3g10940), BE2 (At5g03650), BE3 (At2g36390), and ISA1 (At2g39930).

Acknowledgments

The authors acknowledge the group of Prof. Dr. Bernd Müller-Röber (University of Potsdam) for their assistance with the use of Tecan microplate reader and thank Junio Flores Castellanos and Qingting Liu for their assistance with CE-LIF result analysis and plant preparations, respectively.

Author contributions

X.L. and J.F. conceived and designed the experiments; X.L., A.M.A., L.D., and Z.Y. conducted the experiments; X.L. analyzed the data; X.L. and J.F. wrote the manuscript; and J.F. revised the manuscript. All authors read and approved the final manuscript.

Supplementary data

The following materials are available in the online version of this article.

Supplementary Figure S1. Heterogeneous starch granule morphology observation.

Supplementary Figure S2. Different starch-modifying enzyme activities.

Supplementary Figure S3. Calculation of the surface area and volume of large and small granules.

Supplementary Figure S4. Chain-length distribution analysis of soluble glucans by CE-LIF.

Supplementary Figure S5. Starch granule number distribution plot of *dpe2sex4* and the occurrence of large starch granules in chloroplasts.

Funding

This work was supported by the Deutsche Forschungsgemeinschaft DFG-FE 1030/5-1 and 6-1.

Conflict of interest statement. The authors declare that they have no conflict of interests.

Data availability

The data underlying this article are available in the article and in its online supplementary material.

References

Bechtel DB, Zayas I, Kaleikau L, Pomeranz Y. Size-distribution of wheat starch granules during endosperm development. Cereal Chem. 1990:**67**(1):59–63.

Blennow A, Bay-Smidt AM, Olsen CE, Møller BL. Analysis of starch-bound glucose 3-phosphate and glucose 6-phosphate using controlled acid treatment combined with high-performance anion-exchange chromatography. J Chromatogr A. 1998:**829**(1-2): 385–391. https://doi.org/10.1016/S0021-9673(98)00855-3

Blennow A, Engelsen SB. Helix-breaking news: fighting crystalline starch energy deposits in the cell. Trends Plant Sci. 2010:**15**(4): 236–240. https://doi.org/10.1016/j.tplants.2010.01.009

Brust H, Lehmann T, D'Hulst C, Fettke J. Analysis of the functional interaction of arabidopsis starch synthase and branching enzyme isoforms reveals that the cooperative action of SSI and BEs results in glucans with polymodal chain length distribution similar to amylopectin. PLoS One. 2014:**9**(7):e102364. https://doi.org/10.1371/journal.pone.0102364

Bürgy L, Eicke S, Kopp C, Jenny C, Lu KJ, Escrig S, Meibom A, Zeeman SC. Coalescence and directed anisotropic growth of starch granule initials in subdomains of *Arabidopsis thaliana* chloroplasts. Nat Commun. 2021:**12**(1):6944. https://doi.org/10.1038/s41467-021-27151-5

Chen J, Chen Y, Watson-Lazowski A, Hawkins E, Barclay JE, Fahy B, Bowers RD, Corbin K, Warren FJ, Blennow A, et al. The plastidial protein MRC promotes starch granule initiation in wheat leaves but delays B-type granule initiation in the endosperm. bioRxiv 511297. https://doi.org/10.1101/2022.10.07.511297, 31 October 2022, preprint: not peer reviewed.

Chia T, Thorneycroft D, Chapple A, Messerli G, Chen J, Zeeman SC, Smith SM, Smith AM. A cytosolic glucosyltransferase is required for conversion of starch to sucrose in *Arabidopsis* leaves at night. Plant J. 2004:**37**(6):853–863. https://doi.org/10.1111/j.1365-313X.2003.02012.x

Comparot-Moss S, Kotting O, Stettler M, Edner C, Graf A, Weise SE, Streb S, Lue W-L, MacLean D, Mahlow S, et al. A putative phosphatase, LSF1, is required for normal starch turnover in *Arabidopsis* leaves. Plant Physiol. 2010:**152**(2):685–697. https://doi.org/10.1104/pp.109.148981

Compart J, Li X, Fettke J. Starch-A complex and undeciphered biopolymer. J Plant Physiol. 2021:**258–259**:153389. https://doi.org/10.1016/j.jplph.2021.153389

Doner LW, Irwin PL. Assay of reducing end-groups in oligosaccharide homologues with 2,2′-bicinchoninate. Anal Biochem. 1992:**202**(1): 50–53. https://doi.org/10.1016/0003-2697(92)90204-K

Dumez S, Wattebled F, Dauvillee D, Delvalle D, Planchot V, Ball SG, D'Hulst C. Mutants of *Arabidopsis* lacking starch branching enzyme II substitute plastidial starch synthesis by cytoplasmic maltose accumulation. Plant Cell. 2006:**18**(10):2694–2709. https://doi.org/10.1105/tpc.105.037671

Esch L, Ngai QY, Barclay JE, Seung D (2022) AtFZL is required for correct starch granule morphology in *Arabidopsis* chloroplasts. bioRxiv 512996. https://doi.org/10.1101/2022.10.20.512996, 21 October 2022, preprint: not peer reviewed.

Fettke J, Eckermann N, Tiessen A, Geigenberger P, Steup M. Identification, subcellular localization and biochemical characterization of water-soluble heteroglycans (SHG) in leaves of *Arabidopsis thaliana* L.: distinct SHG reside in the cytosol and in the apoplast. Plant J. 2005:**43**(4):568–585. https://doi.org/10.1111/j.1365-313X.2005.02475.x

Fettke J, Leifels L, Brust H, Herbst K, Steup M. Two carbon fluxes to reserve starch in potato (*Solanum tuberosum* L.) tuber cells are closely interconnected but differently modulated by temperature. J Exp Bot. 2012:**63**(8):3011–3029. https://doi.org/10.1093/jxb/ers014

Fettke J, Malinova I, Albrecht T, Hejazi M, Steup M. Glucose-1-phosphate transport into protoplasts and chloroplasts from leaves of *Arabidopsis*. Plant Physiol. 2011:**155**(4):1723–1734. https://doi.org/10.1104/pp.110.168716

Fujita N, Yoshida M, Asakura N, Ohdan T, Miyao A, Hirochika H, Nakamura Y. Function and characterization of starch synthase I using mutants in rice. Plant Physiol. 2006:**140**(3):1070–1084. https://doi.org/10.1104/pp.105.071845

Grange RI, Hammond JBW, Andrews J. Characteristics of starch grains isolated from mature pepper leaves grown under different irradiances and daylengths. J Exp Bot. 1989:**40**(9):1045–1052. https://doi.org/10.1093/jxb/40.9.1045

Hejazi M, Fettke J, Haebel S, Edner C, Paris O, Frohberg C, Steup M, Ritte G. Glucan, water dikinase phosphorylates crystalline maltodextrins and thereby initiates solubilization. Plant J. 2008:**55**(2):323–334. https://doi.org/10.1111/j.1365-313X.2008.03513.x

Hejazi M, Fettke J, Kötting O, Zeeman SC, Steup M. The Laforin-like dual-specificity phosphatase SEX4 from *Arabidopsis* hydrolyzes both C6- and C3-phosphate esters introduced by starch-related dikinases and thereby affects phase transition of α-glucans. Plant Physiol. 2010:**152**(2):711–722. https://doi.org/10.1104/pp.109.149914

Hejazi M, Fettke J, Paris O, Steup M. The two plastidial starch-related dikinases sequentially phosphorylate glucosyl residues at the surface of both the A- and B-type allomorphs of crystallized maltodextrins but the mode of action differs. Plant Physiol. 2009:**150**(2):962–976. https://doi.org/10.1104/pp.109.138750

Hejazi M, Fettke J, Steup M. Starch phosphorylation and dephosphorylation: The consecutive action of starch-related dikinases and phosphatases. In: Tetlow IJ, editor. Essential reviews in experimental biology: starch: Origins, Structure and Metabolism. Vol. 5. London: SEB; 2012. p. 279–310.

Hejazi M, Mahlow S, Fettke J. The glucan phosphorylation mediated by α-glucan, water dikinase (GWD) is also essential in the light phase for a functional transitory starch turn-over. Plant Signal Behav. 2014:**9**(7):e28892. https://doi.org/10.4161/psb.28892

Jane J, Chen YY, Lee LF, McPherson AE, Wong KS, Radosavljevic M, Kasemsuwan T. Effects of amylopectin branch chain length and amylose content on the gelatinization and pasting properties of starch. Cereal Chem. 1999:**76**(5):629–637. https://doi.org/10.1094/CCHEM.1999.76.5.629

Konik-Rose C, Thistleton J, Chanvrier H, Tan I, Halley P, Gidley M, Kosar-Hashemi B, Wang H, Larroque O, Ikea J, et al. Effects of starch synthase IIa gene dosage on grain, protein and starch in endosperm of wheat. Theor Appl Genet. 2007:**115**(8):1053–1065. https://doi.org/10.1007/s00122-007-0631-0

Kötting O, Santelia D, Edner C, Eicke S, Marthaler T, Gentry MS, Comparot-Moss S, Chen J, Smith AM, Steup M, et al. STARCH-EXCESS4 Is a Laforin-like phosphoglucan phosphatase required for starch degradation in *Arabidopsis thaliana*. Plant Cell. 2009:**21**(1):334–346. https://doi.org/10.1105/tpc.108.064360

Langeveld SMJ, van Wijk R, Stuurman N, Kijne JW, de Pater S. B-type granule containing protrusions and interconnections between amyloplasts in developing wheat endosperm revealed by transmission electron microscopy and GFP expression. J Exp Bot. 2000:**51**(349): 1357–1361. https://doi.org/10.1093/jexbot/51.349.1357

Li X, Apriyanto A, Castellanos JF, Compart J, Muntaha SN, Fettke J. Dpe2/phs1 revealed unique starch metabolism with three distinct phases characterized by different starch granule numbers per chloroplast, allowing insights into the control mechanism of granule number regulation by gene co-regulation and metabolic profiling. Front. Plant Sci. 2022:**13**:1039534. https://doi.org/10.3389/fpls.2022.1039534

Liu Q, Li X, Fettke J. Starch granules in *Arabidopsis thaliana* mesophyll and guard cells show similar morphology but differences in size and number. Int J Mol Sci. 2021:**22**(11):5666. https://doi.org/10.3390/ijms22115666

Lu K-J, Streb S, Meier F, Pfister B, Zeeman SC. Molecular genetic analysis of glucan branching enzymes from plants and bacteria in *Arabidopsis* reveals marked differences in their functions and capacity to mediate starch granule formation. Plant Physiol. 2015:**169**(3):1638–1655. https://doi.org/10.1104/pp.15.00792

Mahlow S, Hejazi M, Kuhnert F, Garz A, Brust H, Baumann O, Fettke J. Phosphorylation of transitory starch by α-glucan, water dikinase during starch turnover affects the surface properties and morphology of starch granules. New Phytol. 2014:**203**(2):495–507. https://doi.org/10.1111/nph.12801

Mahlow S, Orzechowski S, Fettke J. Starch phosphorylation: insights and perspectives. Cell Mol Life Sci. 2016:**73**(14):2753–2764. https://doi.org/10.1007/s00018-016-2248-4

Malinova I, Alseekh S, Feil R, Fernie AR, Baumann O, Schöttler MA, Lunn JE, Fettke J. Starch synthase 4 and plastidal phosphorylase differentially affect starch granule number and morphology. Plant Physiol. 2017:**174**(1):73–85. https://doi.org/10.1104/pp.16.01859

Malinova I, Fettke J. Reduced starch granule number per chloroplast in the dpe2/phs1 mutant is dependent on initiation of starch degradation. PLoS One. 2017:**12**(11):e0187985. https://doi.org/10.1371/journal.pone.0187985

Malinova I, Mahto H, Brandt F, AL-Rawi S, Qasim H, Brust H, Hejazi M, Fettke J. EARLY STARVATION1 specifically affects the phosphorylation action of starch-related dikinases. Plant J. 2018:**95**(1):126–137. https://doi.org/10.1111/tpj.13937

Malinova I, Qasim HM, Brust H, Fettke J. Parameters of starch granule genesis in chloroplasts of *Arabidopsis thaliana*. Front Plant Sci. 2018:**9**:761. https://doi.org/10.3389/fpls.2018.00761

Mérida A, Fettke J. Starch granule initiation in *Arabidopsis thaliana* chloroplasts. Plant J. 2021:**107**(3):688–697. https://doi.org/10.1111/tpj.15359

Mikkelsen R, Baunsgaard L, Blennow A. Functional characterization of alpha–glucan,water dikinase, the starch phosphorylating enzyme. Biochem J. 2004:**377**(2):525–532. https://doi.org/10.1042/bj20030999

Nakamura Y, Francisco PB, Hosaka Y, Sato A, Sawada T, Kubo A, Fujita N. Essential amino acids of starch synthase IIa differentiate amylopectin structure and starch quality between *japonica* and *indica* rice varieties. Plant Mol Biol. 2005:**58**(2):213–227. https://doi.org/10.1007/s11103-005-6507-2

Niittylä T, Comparot-Moss S, Lue W-L, Messerli G, Trevisan M, Seymour MDJ, Gatehouse JA, Villadsen D, Smith SM, Chen J, et al. Similar protein phosphatases control starch metabolism in plants and glycogen metabolism in mammals. J Biol Chem. 2006:**281**(17):11815–11818. https://doi.org/10.1074/jbc.M600519200

Parker ML. The relationship between A-type and B-type starch granules in the developing endosperm of wheat. J Cereal Sci. 1985:**3**(4):271–278. https://doi.org/10.1016/S0733-5210(85)80001-1

Pfister B, Zeeman SC. Formation of starch in plant cells. Cell Mol Life Sci. 2016:**73**(14):2781–2807. https://doi.org/10.1007/s00018-016-2250-x

Ritte G, Heydenreich M, Mahlow S, Haebel S, Kötting O, Steup M. Phosphorylation of C6- and C3-positions of glucosyl residues in starch is catalysed by distinct dikinases. FEBS Lett. 2006:**580**(20):4872–4876. https://doi.org/10.1016/j.febslet.2006.07.085

Ritte G, Scharf A, Eckermann N, Haebel S, Steup M. Phosphorylation of transitory starch is increased during degradation. Plant Physiol. 2004:**135**(4):2068–2077. https://doi.org/10.1104/pp.104.041301

Samodien E, Jewell JF, Loedolff B, Oberlander K, George GM, Zeeman SC, Damberger FF, van der Vyver C, Kossmann J, Lloyd JR. Repression of Sex4 and like sex four2 orthologs in potato increases tuber starch bound phosphate with concomitant alterations in starch physical properties. Front. Plant Sci. 2018:**9**:1044. https://doi.org/10.3389/fpls.2018.01044

Santacruz S, Koch K, Andersson R, Åman P. Characterization of potato leaf starch. J Agric Food Chem. 2004:**52**(7):1985–1989. https://doi.org/10.1021/jf030601k

Santelia D, Kötting O, Seung D, Schubert M, Thalmann M, Bischof S, Meekins DA, Lutz A, Patron N, Gentry MS, et al. The phosphoglucan phosphatase like sex four2 dephosphorylates starch at the C3-position in *Arabidopsis*. Plant Cell. 2011:**23**(11):4096–4111. https://doi.org/10.1105/tpc.111.092155

Seung D, Boudet J, Monroe J, Schreier TB, David LC, Abt M, Lu K-J, Zanella M, Zeeman SC. Homologs of PROTEIN TARGETING TO STARCH control starch granule initiation in *Arabidopsis* leaves. Plant Cell. 2017:**29**(7):1657–1677. https://doi.org/10.1105/tpc.17.00222

Seung D, Smith AM. Starch granule initiation and morphogenesis—progress in *Arabidopsis* and cereals. J Exp Bot. 2019:**70**(3):771–784. https://doi.org/10.1093/jxb/ery412

Sokolov LN, Dominguez-Solis JR, Allary A-L, Buchanan BB, LuanS. A redox-regulated chloroplast protein phosphatase binds to starch diurnally and functions in its accumulation. Proc Natl Acad Sci. 2006:**103**(25):9732–9737. https://doi.org/10.1073/pnas.0603329103

Streb S, Delatte T, Umhang M, Eicke S, Schorderet M, Reinhardt D, Zeeman SC. Starch granule biosynthesis in *Arabidopsis* is abolished by removal of all debranching enzymes but restored by the subsequent removal of an endoamylase. Plant Cell. 2008:**20**(12):3448–3466. https://doi.org/10.1105/tpc.108.063487

Streb S, Zeeman SC. Starch metabolism in Arabidopsis. Arabidopsis Book. Vol. 10. 2012. e0160.

Szydlowski N, Ragel P, Raynaud S, Lucas MM, Roldán I, Montero M, Muñoz FJ, Ovecka M, Bahaji A, Planchot V, et al. Starch granule initiation in *Arabidopsis* requires the presence of either class IV or class III starch synthases. Plant Cell. 2009:**21**(8):2443–2457. https://doi.org/10.1105/tpc.109.066522

Vandromme C, Spriet C, Dauvillée D, Courseaux A, Putaux J-L, Wychowski A, Krzewinski F, Facon M, D'Hulst C, Wattebled F. PII1: a protein involved in starch initiation that determines granule number and size in *Arabidopsis* chloroplast. New Phytol. 2019:**221**(1):356–370. https://doi.org/10.1111/nph.15356

Wattebled F, Dong Y, Dumez S, Delvallé D, Planchot V, Berbezy P, Vyas D, Colonna P, Chatterjee M, Ball S, et al. Mutants of *Arabidopsis* lacking a chloroplastic isoamylase accumulate phytoglycogen and an abnormal form of amylopectin. Plant Physiol. 2005:**138**(1):184–195. https://doi.org/10.1104/pp.105.059295

Xu X, Dees D, Dechesne A, Huang X-F, Visser RGF, Trindade LM. Starch phosphorylation plays an important role in starch biosynthesis. Carbohydr Polym. 2017:**157**:1628–1637. https://doi.org/10.1016/j.carbpol.2016.11.043

Zeeman SC, Kossmann J, Smith AM. Starch: its metabolism, evolution, and biotechnological modification in plants. Annu Rev Plant Biol. 2010:**61**(1):209–234. https://doi.org/10.1146/annurev-arplant-042809-112301

Zeeman SC, Tiessen A, Pilling E, Kato KL, Donald AM, Smith AM. Starch synthesis in *Arabidopsis*. Granule synthesis, composition, and structure. Plant Physiol. 2002:**129**(2):516–529. https://doi.org/10.1104/pp.003756

Zhu A, Romero R, Petty HR. An enzymatic colorimetric assay for glucose-6-phosphate. Anal Biochem. 2011:**419**(2):266–270. https://doi.org/10.1016/j.ab.2011.08.037

Zhong Y, Li Z, Qu J, Bertoft E, Li M, Zhu F, Blennow A, Liu X. Relationship between molecular structure and lamellar and crystalline structure of rice starch. Carbohydr Polym. 2021:**258**:117616. https://doi.org/10.1016/j.carbpol.2021.117616